THE JOURNAL OF PHYSICAL CHEMISTRY C
A JOURNAL OF THE AMERICAN CHEMICAL SOCIETY

pubs.acs.org/JPCC

Article

Computational Investigation of Structure–Function Relationship in Fluorine-Functionalized MOFs for PFOA Capture from Water

Turan Selman Erkal, Norazanita Shamsuddin, Serdal Kirmizialtin, and A. Ozgur Yazaydin*

Cite This: J. Phys. Chem. C 2023, 127, 3204–3216

Read Online

ACCESS | Metrics & More | Article Recommendations | Supporting Information

ABSTRACT: A strategy that can be used to develop metal–organic frameworks (MOFs) to capture per- and poly-fluoroalkyl substances (PFAS) from water is functionalizing them with fluorine moieties. We investigated different fluorine-functionalization strategies and their performance in removing PFAS from water using molecular simulations. Perfluorooctanoic acid (PFOA), one of the most widely encountered PFAS in water sources, was used as the probe molecule. Our simulations show that fluorine functionalization by incorporating fluorinated anions as bridging ligands in MOFs creates additional binding sites for PFOA; however, the same sites also attract water molecules, which casts doubt on their potential use. In contrast, trifluoromethyl or fluorine substitution of the MOF ligands results in higher hydrophobicity. However, the pores fluorinated with this method should have the optimum size to accommodate PFOA. Likewise, post-synthetic fluorine functionalization of MOFs through grafting of perfluorinated alkanes showed increased PFOA affinity. Fluorine-functionalized MOFs with high hydrophobicity and optimized pore sizes can effectively capture PFOA from water at very low concentrations of PFOA.

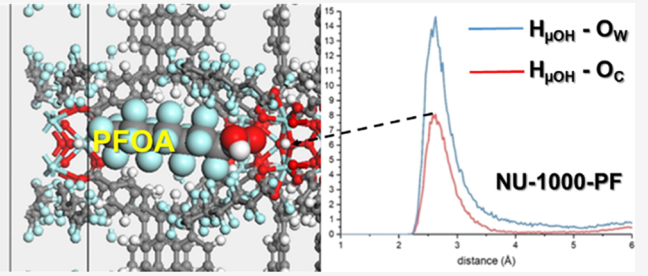

1. INTRODUCTION

The release of toxic chemicals into the environment, whether accidental or due to their utilization in industries, has inevitably led to the contamination of soil, surface water, and ground water.[1,2] One group of pollutants that has attracted a great deal of attention recently is per- and polyfluoroalkyl substances (PFAS) which are found through point sources—e.g., wastewater treatment plants (WWTPs), landfills, PFAS manufacturing units, fluorine industries, and fire-fighting training areas—and non-point sources—e.g., household products, food packaging, wet and dry depositions of the atmosphere, and surface runoffs.[3−5] PFAS are known to be highly resistant to degradation and decomposition due to the presence of strong carbon-fluorine covalent bonds. As such, they are ideal for use in harsh conditions.[6] The chemical and thermal stabilities of PFAS also mean that they do not break down easily in nature; as such, they are referred to as "forever chemicals". They can be found in soil particles, porous substrates, and groundwater runoffs, polluting agricultural soil and freshwater sources.[7] Thus, PFAS can easily contaminate soil and eventually get into the groundwater, where it may end up in food chain resources.[6−11] They have even been found in bottled drinking water, tea, and juice samples[12] and drinking water.[13−16] A new study reports that PFAS exceeds the United States Environmental Protection Agency advisory levels in rainwater and snow worldwide.[17] Toxicology tests carried out on human urine and serum samples detected concerning amounts of PFAS.[18]

These persistent industrial chemical wastes are toxic to living beings. Human and animal studies of PFAS revealed that these substances could lead to neurological, liver, and lung problems and disrupt hormonal balance.[19−22] Additionally, the cancerous effect of PFAS was investigated, and results indicate that PFAS exposure increases the risk of getting kidney and testicular cancer.[23,24] Epidemiological studies have also shown that exposure to specific PFAS has several health effects: immunosuppression among children, adolescents, and adults as well as other targeted organs such as the placenta in pregnant women;[24] there is also sufficient proven evidence indicating that PFAS exposure would affect breast milk production and breastfeeding duration.[25−27] There are also findings linking PFAS with elevated cholesterol levels and significant birth defects.[28,29]

Typically, analysis of PFAS can be performed using a targeted quantitative method, e.g., high-performance liquid chromatography (HPLC) with tandem mass spectrometry (MS). However, such a method is limited to the referenced PFAS in the literature. The emergence of more reliable methods, i.e., suspect screenings and non-targeted analyses

Received: November 3, 2022
Revised: January 17, 2023
Published: February 3, 2023

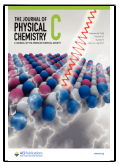

(NTA), has improved the level of coverage in identifying new emerging PFAS and enhanced our knowledge of their distribution.[29] New methods are used to identify new PFAS and their isomers in aqueous samples, such as COnductor-like Screening MOdel for Real-Solvents (COSMO-RS)[30] and in silico PFAS fragmentation modeling[31] together with data mining software.[32]

The removal of PFAS from water has been investigated extensively due to their potentially harmful effects. Biological degradation of PFAS with fungal enzymes and microorganisms or their removal with phytoremediation is simple, cost-effective, and environmentally friendly yet requires several months to work.[33] Degradation of PFAS in water with oxidation processes, i.e., chemical, photochemical, or ultrasonic, can be an effective method, but scaling up of oxidation processes for the removal of large amounts of PFAS is not trivial.[33−35] Membrane filtration is another technology that can be utilized for PFAS removal. Microfiltration (MF) and ultrafiltration (UF) may not be suitable for rejecting low-molecular weight PFAS compounds. Still, these membranes can be helpful during pretreatment to concentrate PFAS and control fouling. High-pressure membrane processes such as reverse osmosis (RO) and nanofiltration (NF) membranes and other techniques could improve PFAS removal, e.g., UF-RO treatment removed >99% PFAS from water.[36] However, to date, most membrane studies were done on a lab/pilot scale and hence lacked the field application data.[7] Another method to remove PFAS from water is coagulation. Several coagulants, such as alum and iron salts, have been employed to precipitate PFAS in water.[33,37,38] While coagulation is an effective method, difficulties in controlling agglomeration and the possibility of side reactions present challenges for its large-scale application for PFAS removal. In addition to the methods mentioned above, PFAS can also be removed from water by adsorbents.

As one of the cheapest and simplest adsorbents, activated carbon (AC), already used for water remediation and filtering applications in powdered and granular form, has been tested for PFAS removal and is often considered a benchmark material.[33,37,38] Other carbon-based adsorbents, such as carbon nanotubes (CNTs) and graphene, have higher specific surface areas, porosity, and adsorption capacity; hence, they have better PFAS removal performance compared to AC, yet these methods are more expensive.[39] Ion exchange resins capture PFAS through electrostatic and hydrophobic interactions,[4,38−40] and some showed better PFAS capture performance compared to AC.[38,39] However, regeneration of the ion exchange resins has been a formidable issue that still needs to be addressed.[4,38,41] Other polymeric materials such as polyaniline nanotube (PANT), which is more porous than resin polymers, demonstrated high affinity to PFOA and perfluorooctanesulfonic acid (PFOS) when they are in their anionic forms in low-pH solutions.[33,42,43] Polymer networks that contain macrocyclic hosts such as calixarene or β-cyclodextrin have shown promising performance for capturing PFAS from water.[43−45] Zeolites and crystalline and microporous materials have been studied experimentally and computationally for PFAS removal from water.[46,47] In particular, zeolite Beta showed faster adsorption kinetics and larger uptake than AC.[46]

Covalent organic frameworks (COFs) and organic metal frameworks (MOFs) are porous crystalline structures similar to zeolites. Amine-functionalized, triazine-based, and cationic forms of COFs have been used as PFAS removal agents from water.[48−50] Likewise, MOFs such as ZIF-7, ZIF-8, UiO-66, MIL-101(Cr), and NU-1000 have been considered for PFAS removal, and their performance was studied experimentally.[51−54]

Previous studies have shown that fluorine functionalization can improve the adsorptive removal of PFAS from water in porous materials, such as in calixarenes,[44] MOFs,[51] polymers,[55,56] and graphene.[57] MOFs, in particular, offer great prospects because their crystalline porous inorganic−organic nature can be tuned to have the desired pore size, shape, and chemical functionality. They are an ideal platform to investigate and compare fluorine functionalization strategies for PFAS removal from water.

In this work, we investigate MOFs fluorine-functionalized by different strategies to explore their potential for PFAS removal from water using computer simulations. We study perfluorooctanoic acid (PFOA), one of the most widely observed PFAS in groundwater, and analyze specific interactions between the frameworks and the PFOA molecule. Henry's law coefficients computed for PFOA and water in each MOF considered in this study are used as a quantitative measure to assess the performance of each MOF for PFOA removal. We considered 15 MOFs possessing different pore sizes, hydrophobicities, and fluorine functionalization strategies. We find that fluorination, in all cases, improves the performance of MOFs by increasing the framework−PFOA interactions. The performance varied significantly depending on MOF topology and functionalization strategy. We identify the structural and energetic factors that govern Henry's law coefficient, which will guide us to develop better materials to remove PFAS from water.

2. COMPUTATIONAL METHODS

In this study, we considered MOFs fluorine-functionalized by different methods and categorized them following the convention given in Noro et al.[58] based on the fluorine functionalization strategy (Table 1). The first category is

Table 1. Fluorinated MOFs Considered in this Work[j]

fluorine functionalization method	MOF name	formula	ref
fluorinated anion, AF_6^{2-} (A = Si and Ti) bridging ligands	SIFSIX-1-Cu[a] (Cu(bpy-1)$_2$(SiF$_6$))	$C_{20}H_{16}CuN_4SiF_6$	64
	TIFSIX-1-Cu[b] (Cu(bpy-1)$_2$(TiF$_6$))	$C_{20}H_{16}CuN_4TiF_6$	61
	Zn(4,4′-bpy)$_2$(SiF$_6$)[c]	$C_{20}H_{16}ZnN_4SiF_6$	59
	Cu(bpy-2)$_2$(SiF$_6$)[d]	$C_{24}H_{16}CuN_4SiF_6$	62
	SIFSIX-2-Cu[e] (Cu(dpa)$_2$(SiF$_6$))	$C_{24}H_{16}CuN_4SiF_6$	60
trifluoromethyl (-CF$_3$) or fluorine-substituted ligands	Zn($C_{17}H_8F_6O_4$)[f]	$C_{34}H_{16}F_{12}O_8Zn_2$	65
	FMOF-1[g]	$C_{12}Ag_3F_{18}N_9$	66
	F-UiO-67[h]	$C_{42}H_{(26-n)}F_nO_{16}Zr_3$	this work
perfluoraalkane grafting	NU-1000-PF[i]	($C_{44}H_{30}O_{16}Zr_3$) + $C_7F_{15}COO$	68

[a]Detailed structural representations of the MOFs listed in Table 1 are given in the ESI, Figure S1. [b]Figure S2. [c]Figure S3. [d]Figure S4. [e]Figure S5. [f]Figure S6. [g]Figure S7. [h]Figure S8. [i]Figure S9. [j]bpy and py-1 = 4,4′-bipyridine; bpy-2 = 1,2-bis(4-pyridyl)ethene); dpa = 4,4′-dipyridylacetylene

https://doi.org/10.1021/acs.jpcc.2c07737
J. Phys. Chem. C 2023, 127, 3204−3216

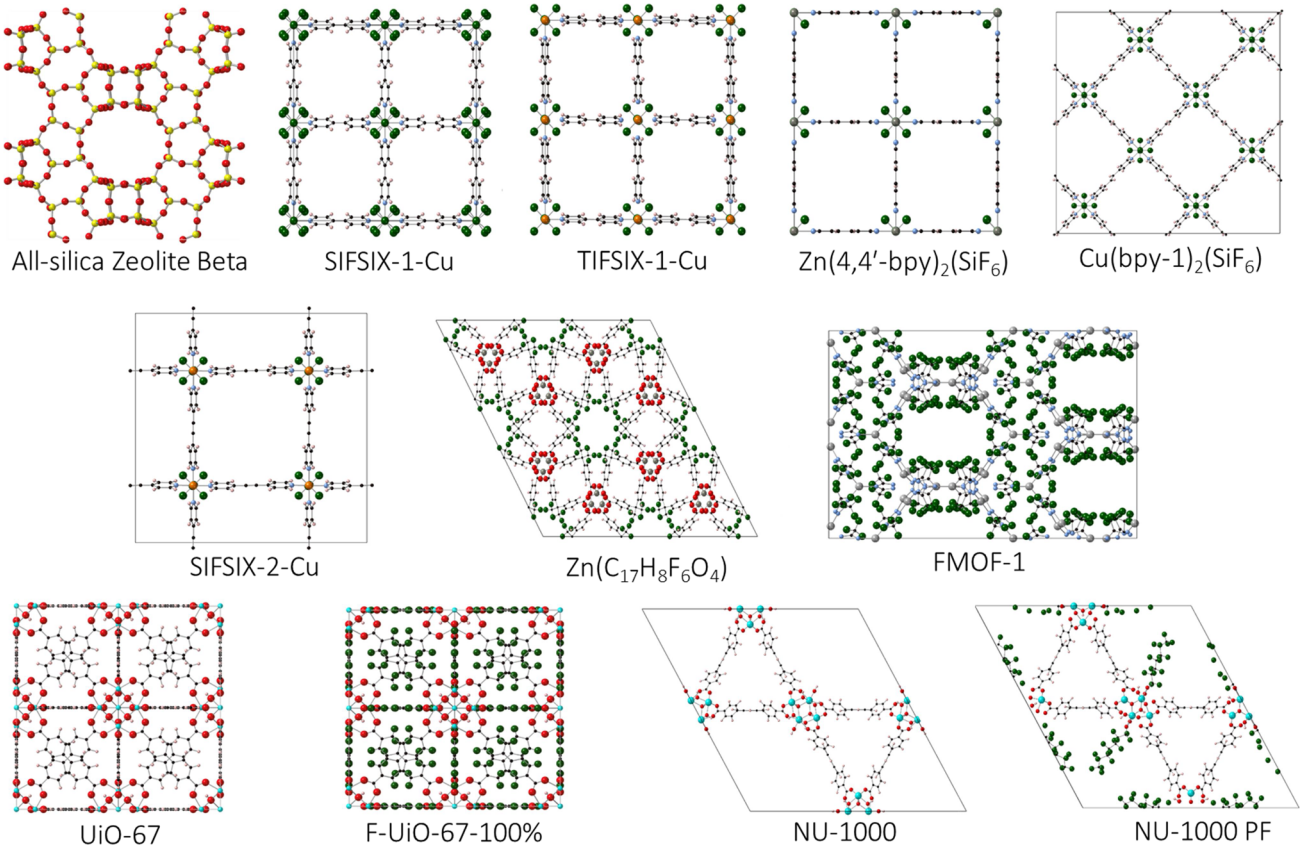

Figure 1. Unit cells of the structures considered in this study. Larger figures of the unit cells and color coding of the atoms can be found in the ESI (Figures S1−S10).

fluorinated anion functionalized MOFs, where AF_6^{2-} anions (A = Si or Ti) are used as bridging ligands.[59−64] The second category is substitution with trifluoromethyl or fluorine.[65,66] The two MOFs considered in this category, FMOF-1[66] and $Zn(C_{17}H_8F_6O_4)$,[65] have trifluoromethyl-substituted ligands. For MOFs with ligands substituted with fluorine atoms, we considered fluorine-functionalized UiO-67, denoted by F-UiO-67. A fluorine-substituted UiO-67 has not been reported experimentally in the literature to the best of our knowledge; however, fluorine-functionalized UiO-66, which has short bridging ligands compared to UiO-67 but has the same topology, was reported experimentally.[67] Therefore, fluorine-functionalized UiO-67 structures were constructed computationally by substituting 25, 50, 75, and 100% of the hydrogens on the linkers with fluorine atoms by following the same incremental fluorine substitution approach employed for UiO-66 experimentally.[67]

The third and last category is MOFs that are fluorine-functionalized by grafting perfluoraalkanes.[68,69] In this category, we considered perfluoro alkane functionalized NU-1000, denoted as NU-1000-PF. NU-1000 is a Zr-based metal−organic framework, and it was fluorine-functionalized by inserting PFOA molecules as charge-compensating moieties to the Zr_6 nodes by employing the solvent-assisted ligand incorporation (SALI) method.[68] Finally, all-silica zeolite Beta, which is hydrophobic and was shown to be a highly selective adsorbent for PFAS, was included in this study as a benchmark material for comparison with fluorinated MOFs.[46,70] Unit cells of the MOFs and zeolite Beta are shown in Figure 1.

2.1. DFT Calculations. The crystal structures of MOFs and all-silica zeolite Beta were obtained from either the Cambridge Crystallographic Data Centre (CCDC)[71] or from the references in Table 1. We employed geometry optimization for each structure using periodic density functional theory (DFT). The DFT calculations were carried out with CASTEP 19.11 software.[72] The PBE functional and ultrasoft pseudopotentials were used with a 550 eV energy cut-off. Partial atomic charges of the geometrically optimized MOF structures were calculated using the REPEAT method.[73] In this method, point charges are fit to reproduce the DFT-derived periodic electrostatic potential of the MOF.

2.2. Force Field. The force field used in the molecular simulations included non-bonded and bonded interactions. Short-range van der Waals interactions and the long-range electrostatic interactions between non-bonded atoms were computed through the Lennard−Jones (LJ) and Coulomb potentials, respectively, with the following equation:

$$V(r_{ij}) = 4\varepsilon_{ij}\left[\left(\frac{\sigma}{r_{ij}}\right)^{12} - \left(\frac{\sigma}{r_{ij}}\right)^{6}\right] + \frac{1}{4\pi\varepsilon_0}\frac{q_i q_j}{r_{ij}}$$

where V is the total energy, i and j are interacting atoms, and r_{ij} is the distance between these atoms. ε_{ij} and σ_{ij} are the well depth and diameter, respectively. q_i and q_j are the partial charges of the interacting atoms, and finally, ε_0 is the dielectric constant in vacuum. LJ parameters between different types of atoms were calculated using Lorentz−Berthelot mixing rules. As described in the previous section, the partial atomic charges of MOF atoms were derived from DFT calculations, and the

https://doi.org/10.1021/acs.jpcc.2c07737
J. Phys. Chem. C 2023, 127, 3204−3216

Table 2. Force Field Parameters for the PFOA Molecule

atom/group	ε/k_B (K)	σ (Å)	charge	Ref.
CF_3	87	4.36	0	77
CF_2	27.5	4.73	0	77
CF_2-(C)	27.5	4.73	0.12	77, 81
C	41	3.9	0.42	81
O=(C)	79	3.05	-0.45	81
O-(H)	93	3.02	-0.46	81
H-(O)	0	0	0.37	81

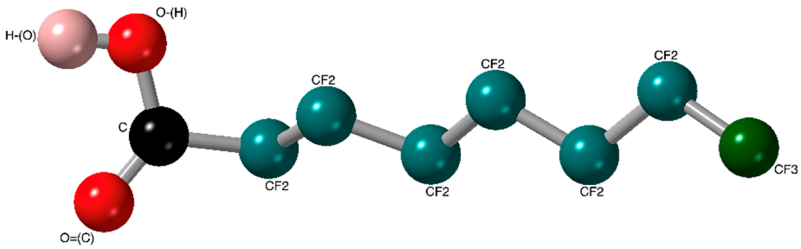

Bond (fixed length)	Length(Å)	Ref	Angle Bend†	θ(deg)	kθ/ k_B(K)	Ref.
CF_3-CF_2	1.54	77	CF_3-(CF_2)-CF_2	114	62500	77
CF_2-CF_2	1.54	77	CF_2-(CF_2)-CF_2	114	62500	77
C=O	1.214	81	H-O-C	107	17600	81
C-O	1.364	81	O-C=O	123	40300	81
O-H	0.97	81	O-C-CF_2	111	35300	81
			O=C-CF_2	126	40300	81

Torsion§	c0	c1	f_1	c2	c3	c4	Ref.
CF_2- CF_2- CF_2- CF_2	0	1666.25	0	247.6	-349.26	-532.94	78
CF_3- CF_2- CF_2- CF_2	0	1666.25	0	247.6	-349.26	-532.94	78
CF_2-CF_2-C=O	2035.58	−736.9	0	57.84	−293.23	0	79
CF_2-CF_2-C-O	0	176.6	0	-53.34	769.93	0	80
CF_2-C-O-H	0	630	0	1562.4	0	0	81
O=C-O-H	0	630	180	1562.4	0	0	81

$^a V(\theta_{ij}) = \frac{(k_\theta)}{2}(\theta - \theta_0)^2$. $^b V(\emptyset) = c_0 + c_1(1 + \cos(\emptyset + f_1)) + c_2(1 - \cos(2\emptyset)) + c_3(1 + \cos(3\emptyset)) + c_4(1 - \cos(4\emptyset))$; 1−4 interactions are zero.

Lennard−Jones parameters for MOF atoms were taken from the UFF force field.[74] For zeolite Beta, Lennard−Jones parameters and partial atomic charges were taken from the TraPPE-zeo force field.[75] The water molecule was represented with the rigid TIP4P-Ew model.[76]

For the PFOA molecule, we developed a new model that treats each CF_3 and CF_2 unit as united atoms, whereas the atoms on the carboxyl group are treated explicitly. Force field parameters for the new PFOA model were derived from previous force fields used for perfluoroalkanes,[77,78] ketones,[79] alcohols,[80] and carboxylic acid[81] and are given in Table 2. To validate the PFOA model, we performed a molecular dynamics (MD) simulation (see the ESI for details) in the isobaric isothermal ensemble (NPT), which reproduced the experimental density of PFOA at 1 atm and 298 K (1.8 g/cm^3).

The protonation state of PFOA highly depends on the environment. PFOA is expected to be in the deprotonated state in hydrophilic environments due to presence of liquid water, whereas near hydrophobic surfaces, it is expected to be in the neutral state. Recent molecular dynamic simulation studies investigating PFOA adsorption in clay minerals[82] and cyclodextrin-based polymers[83] employ deprotonated models of PFOA because these systems are hydrophilic and liquid water is expected to be present in the pores and cavities of such materials. On the other hand, fluorine-functionalized MOFs considered in this study are expected to be hydrophobic (as we show later in the Results and Discussion section based on computed Henry's law coefficients) with no significant amount of water expected in the pores, apart from local water clusters that can form around certain specific binding sites. In support of this argument, experimental data shows that when defects are created in the highly hydrophobic zeolite Beta, PFOA uptake decreases dramatically. This is due to water adsorption by the defect sites.[46] Based on this, we conjecture that PFOA is primarily neutral in the fluorine-functionalized hydrophobic pores and we model it as neutral.

2.3. Monte Carlo Simulations. All Monte Carlo (MC) simulations were performed using the RASPA molecular simulation software.[84] The cut-off distance for the LJ potential and the real part of the Ewald sum, which was used to compute electrostatic interactions, was set to 12 Å. The unit cells of the MOFs and zeolite Beta were replicated such that their shortest side was greater than twice the cut-off distance. We used MC simulations for two purposes: (i) to compute Henry's law coefficients of PFOA and water and (ii) to probe PFOA and water-preferred adsorption sites. Henry's law coefficients of

https://doi.org/10.1021/acs.jpcc.2c07737
J. Phys. Chem. C 2023, 127, 3204−3216

PFOA and water were calculated with Widom's insertion method[85] by sampling at least 10 million random insertions. To probe PFOA and water-preferred adsorption sites, we employed MC simulations in the NVT ensemble. During conformational sampling, we allowed translation, rotation, and reinsertion of a single PFOA or water molecule in the MOFs and zeolite Beta frameworks. We used at least 2 million MC moves to ensure convergence for each simulation. From these simulations, radial distribution functions (RDFs) between specific sites of the adsorbent materials and the PFOA or water were computed. For each system, we conducted 10 independent MC simulations, and the RDFs reported are averages from these independent simulations.

2.4. Henry's Law Coefficients and Preferred Adsorption Sites of PFOA and Water in Fluorinated MOFs and Zeolite Beta. Because the PFOA concentrations detected in water resources are usually at extremely low,[38,39,86−89] it can be safely assumed that the solubility of PFOA obeys Henry's law at these conditions. Calculation of Henry's law coefficient (HLC) is straightforward and computationally cheap, and it can be a powerful tool to assess the role of pore size, geometry, and chemical functionality on the performance of material for PFOA removal. In our earlier work, we showed that HLC is a useful metric to assess the PFOA removal capacities from water.[44] An ideal material should have a high HLC for PFOA and, at the same time, a low HLC for water, i.e., hydrophobic. Thus, in our comparisons, we used the HLC ratio, R_H = HLC_{PFOA}/HLC_{water}, where HLC_x is the Henry's Law coefficient of PFOA or water, to quantitatively rank the MOFs for PFOA removal. The preferred adsorption sites were revealed by pair distribution functions, i.e., RDF, between specific atoms of the sorbate molecules and the adsorbent material. Topology analysis of the MOFs and zeolite Beta is done by computing pore size distribution with Poreblazer v4.0 software.[90]

To establish structure−function relationships for the PFOA removal of fluorine-functionalized MOFs, we analyzed the MOF topologies and their interactions using pore size distributions (PSD) in conjunction with radial distribution functions (RDF). The first one reports the geometric features that dictated the adsorption; the latter provides information on the energetics of the interactions between the specific sites on the host and guest molecules. In PFOA adsorption, both electrostatic and hydrophobic interactions can play a role.[44] The electrostatic interactions are mostly due to the interaction of the carboxyl group of PFOA and the porous material. In contrast, the hydrophobic interactions occur due to the interaction of the perfluoroalkyl chain of PFOA with the porous material. However, it is the electrostatic interactions that are expected to give distinct peaks in RDF plots indicative of the preferred adsorption sites.

3. RESULTS AND DISCUSSION

To derive structure−function relationships between fluorine-functionalized MOF materials for PFOA removal from water, we studied 15 materials. The materials are selected with varying pore sizes, chemical compositions, and fluorination strategies. Figure 1 displays the structure of the materials under study. In Table 3, we provide details of the individual HLC values for water and PFOA in each system. We plot in Figure 2 the ratio of the Henry Law coefficient ratio (R_H) of PFOA and water for all systems studied.

Table 3. Henry's Law Coefficients of PFOA and Water in MOFs and Zeolites under Study[a]

MOF name	PFOA (mol/kgPa)	water (mol/kgPa)
zeolite Beta	$3.4(3) \times 10^{4}$	$1.711(7) \times 10^{-6}$
SIFSIX-1-Cu	$6(1) \times 10^{5}$	$2.8(4) \times 10^{-3}$
TIFSIX-1-Cu	$1.9(7) \times 10^{6}$	$3.1(7) \times 10^{-3}$
$Zn(4,4'\text{-bpy})_2(SiF_6)$	$3.9(7) \times 10^{6}$	$1.6(5) \times 10^{-3}$
$Cu(bpy\text{-}2)_2(SiF_6)$	$4.6(6) \times 10^{4}$	$4.1(7) \times 10^{-3}$
SIFSIX-2-Cu	$3.4(9) \times 10^{3}$	$1.2(3) \times 10^{-3}$
$Zn(C_{17}H_8F_6O4)$	$2.6(3) \times 10^{-1}$	$1.67(1) \times 10^{-6}$
FMOF-1	4.2(6)	$4.52(3) \times 10^{-7}$
UiO-67	$9.7(4) \times 10^{2}$	$3.9(2) \times 10^{-6}$
F-UiO-67-25%	$1.6(3) \times 10^{3}$	$4.31(2) \times 10^{-6}$
F-UiO-67-50%	$2.2(7) \times 10^{3}$	$4.62(3) \times 10^{-6}$
F-UiO-67-75%	$3.1(7) \times 10^{3}$	$4.9(2) \times 10^{-6}$
F-UiO-67-100%	$4.3(7) \times 10^{3}$	$5.3(1) \times 10^{-6}$
NU-1000	$3.09(7) \times 10^{4}$	$4.18(9) \times 10^{-6}$
NU-1000-PF	$1.7(3) \times 10^{5}$	$3.8(9) \times 10^{-6}$

[a]The values in parenthesis show the statistical uncertainty of the final digit.

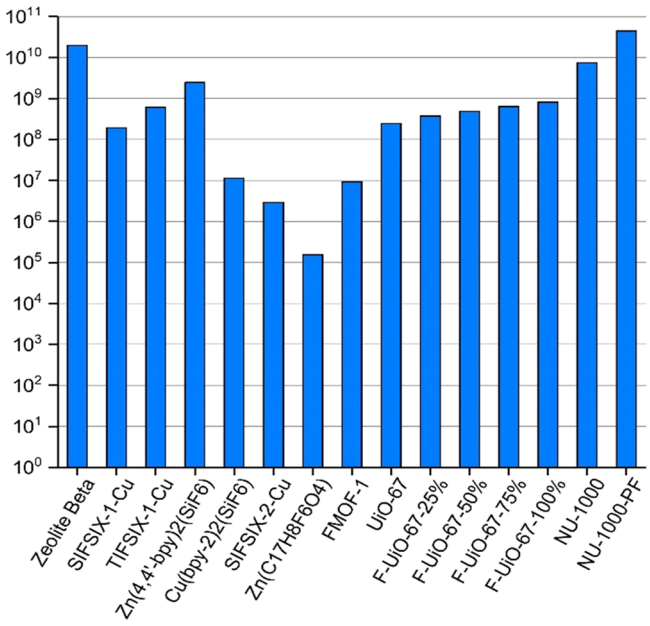

Figure 2. Ratio of PFOA to Water Henry's Law coefficients (R_H).

3.1. Assessment of Strategy with Zeolite Beta. To assess the accuracy of the set criteria of R_H, we study a system known for good PFOA removal performance. Zeolites are crystalline porous materials that have been extensively used in adsorption processes. All-silica zeolite Beta has shown high PFOA removal from water in experimental studies,[46] providing an excellent benchmark system to assess our computational methodology. We computed the HLC of PFOA and water in zeolite Beta (Table 3). The HLC of water shows a low value. In contrast, the HLC of PFOA is very high. The R_H value of 1.9×10^{-10} will be our criteria for other materials.

To understand what makes zeolite beta show a high R_H value, we looked at the PSDs and RDFs. Zeolite beta shows a pore size distribution peaking at 5.8 Å (Figure 3). The RDFs, on the other hand, show no preferred adsorption sites (Figure 4). At the same time, we observe strong hydrophobic properties for water. Taken together, the high performance

https://doi.org/10.1021/acs.jpcc.2c07737
J. Phys. Chem. C 2023, 127, 3204−3216

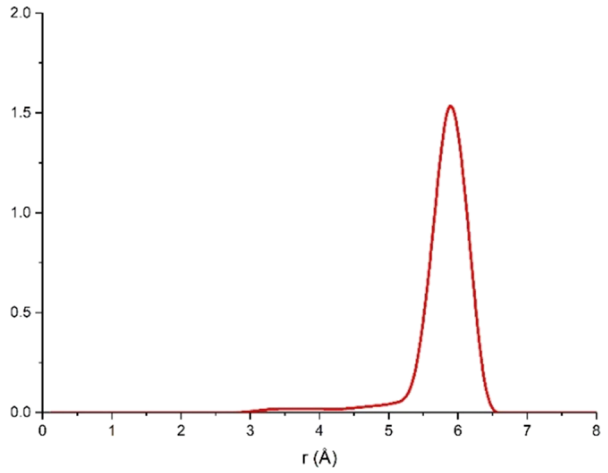

Figure 3. PSD plot of zeolite Beta.

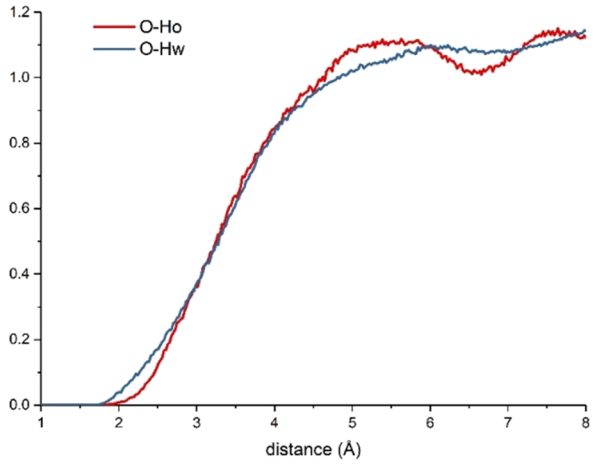

Figure 4. RDF plots in zeolite Beta. O, oxygen atoms of zeolite Beta; H_O, hydrogen atom of PFOA; and H_W, hydrogen atoms of water.

of zeolite Beta can be inferred due to the strong hydrophobicity of the framework and its pore size in which PFOA molecules perfectly fit.

3.2. Impact of Fluorination on the Interactions of MOF with PFOA. To elucidate the impact of fluorination on MOF materials, we study UiO-67. We functionalize this MOF with fluorine-substituted ligands. The fluorination was done incrementally, and its impact on the HLC, PSD, and RDF was monitored. In Figure 2 and Table 3, we show how R_H values change when UiO-67 is gradually fluorine-functionalized, i.e., F-UiO-67-*n*%, where *n* is 25, 50, 75, and 100 percentages of functionalization. We observe that the fluorine substitution increases the R_H approximately four times, going from the non-fluorinated UiO-67 to the fully fluorinated F-UiO-67-100%. The higher the fluorine content, the higher the R_H (Figure 2). We looked at what happens to the pores during fluorine substitution. The PSD plots show the bimodal distribution in UiO-67 (Figure 5). Upon substitution, only subtle changes happened. The fluorination mostly impacts the larger pores. The HLCs of water in all structures are all in the order of 10^{-6} mol/kgPa and increase marginally by about 35% from the non-fluorinated UiO-67 to fully fluorinated F-UiO-67-100%. Although UiO-67 should become more and more hydrophobic due to increasing fluorine content, the small increase in HLC of water may be attributed to the pores becoming slightly

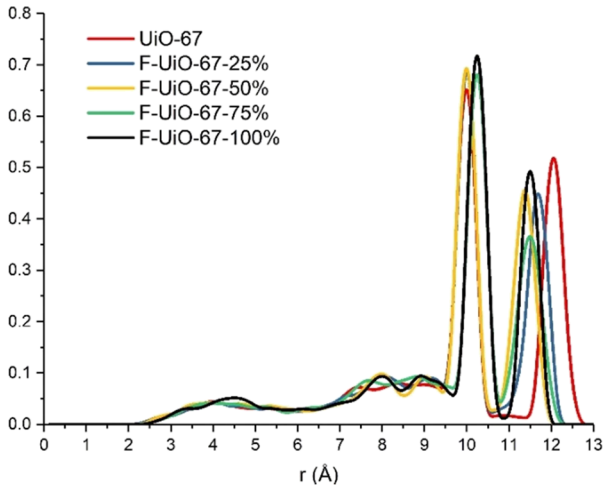

Figure 5. PSD plots of UiO-67 and fluorine-functionalized F-UiO-67s with different degrees of fluorine substitution.

narrower, hence the stronger framework−water interactions. On the other hand, the HLCs of PFOA are in the order of 10^3 mol/kgPa, and the fluorine functionalization of ligands has a significant effect on PFOA HLCs.

To investigate the specific interactions between the MOFs and ligands, we analyzed the RDF plots. RDF plots in UiO-67 and F-UiO-67s that have different degrees of fluorine functionalization provide insights about the preferred adsorption sites of PFOA and water molecules (Figure 6 and Figure S12). Both PFOA and water molecules strongly interact with the hydrogens of μOH sites in UiO-67 and F-UiO-67s (Figure S11, RDF plots for $H_{\mu OH}$-O_C and $H_{\mu OH}$-O_W), that is, PFOA and water compete for the same adsorption site. Once fluorinated, however, a distinct adsorption site is created for the PFOA molecule. In Figure 6a, the RDF plots of the hydrogen atoms of the ligands and the hydroxyl oxygen of PFOA (H-O_H) and the oxygen atoms of water (H-O_W) show that the hydrogens on the MOF ligands are not preferred adsorption sites. However, the RDF plots between the fluorine atoms of F-UiO-67s and hydrogen atom of PFOA (F-H_O) show sharp peaks at around 2.5 Å (Figure 6b−e), indicating the creation of new binding sites on the ligand. Here, the hydrogens of water molecules do not bind to the fluorine atoms of the ligands (RDF plots for F-H_W in Figure 6b−e). As such, the increase in the PFOA affinity in UiO-67 with increasing fluorine substitution of UiO-67 ligands may be attributed to the introduction of distinct adsorption sites for PFOA. Overall, our results demonstrate the impact of fluorination, that is, increasing fluorination of UiO-67 results in increasing R_H values. In the rest of this section, we present the results by grouping the MOFs based on the fluorine functionalization method used in their synthesis.

3.3. MOFs Functionalized with Fluorinated Anions. HLCs of water in MOFs functionalized with fluorinated anions show relatively lower hydrophobicities than other MOFs (Table 3). In contrast, HLCs of PFOA are six to nine orders of magnitude higher than water, favoring PFOA adsorption (Table 3). Based on our set criteria, we find that TIFSIX-1-Cu and $Zn(4,4'4'\text{-bpy})_2(SiF_6)$ show the best performance among this type of MOFs (Figure 2).

Pore size distributions of these MOFs show a unimodal shape with pore sizes ranging between 7.5 Å for SIFSIX-1-Cu to 11 Å for SIFSIX-2-Cu (Figure 7). To understand the role of

https://doi.org/10.1021/acs.jpcc.2c07737
J. Phys. Chem. C 2023, 127, 3204−3216

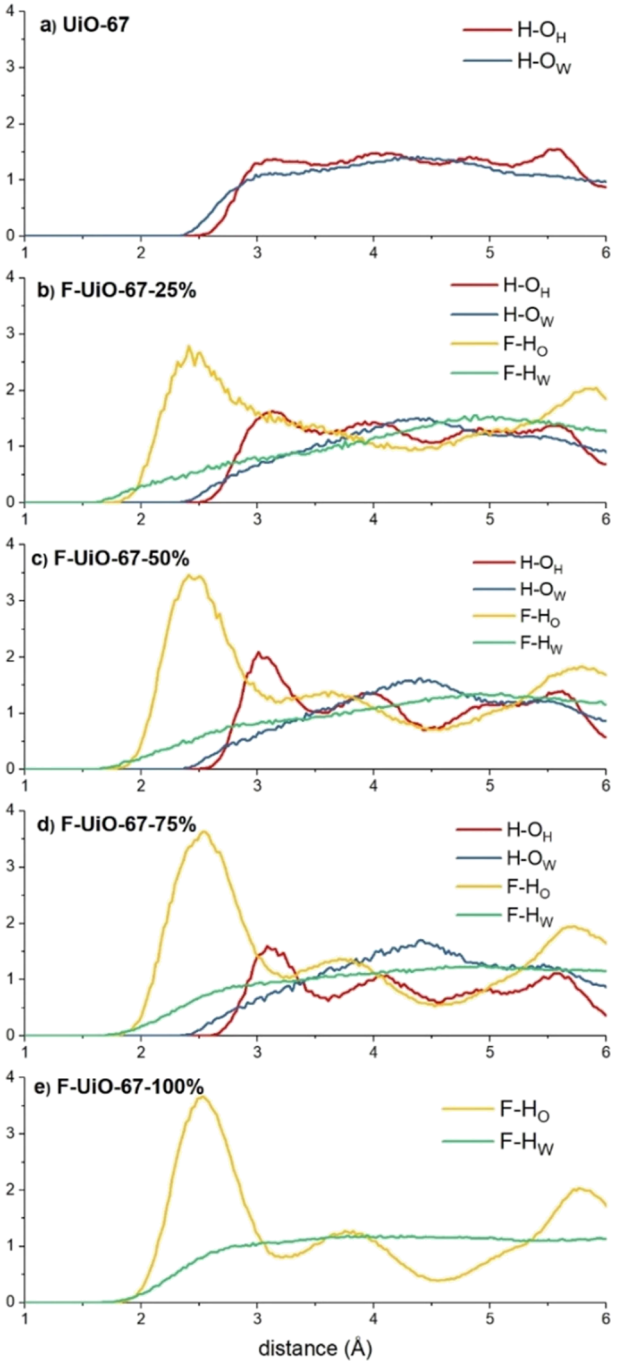

Figure 6. (a–e) RDF plots in UiO-67 and fluorine-functionalized F-UiO-67s with different degrees of fluorine substitution. H, hydrogen atoms on the ligands of UiO-67 and F-UiO-67-25%, 50%, and 75%; F, fluorine atoms of the F-UiO-67s; H_O, hydrogen atom of PFOA; O_H, oxygen atom of PFOA bonded to hydrogen; H_W, hydrogen atoms of water; and O_W, oxygen atom of water. See Figures S12 and S13 for snapshots from simulations that illustrate the interactions between atom pairs for which RDF plots are shown in Figure 6. See Table S1 for the location of the peak centers for the RDF plots given here.

chemical composition on PFOA adsorption, we analyzed preferred adsorption sites by comparing RDFs between MOF framework atoms and the guest molecules. We computed the RDFs of hydrogen atoms of PFOA (F-H_O) to the MOF fluorine atoms and compared this with MOF fluorine–water hydrogens (F-H_W) (Figure 8). Interestingly, for all MOFs

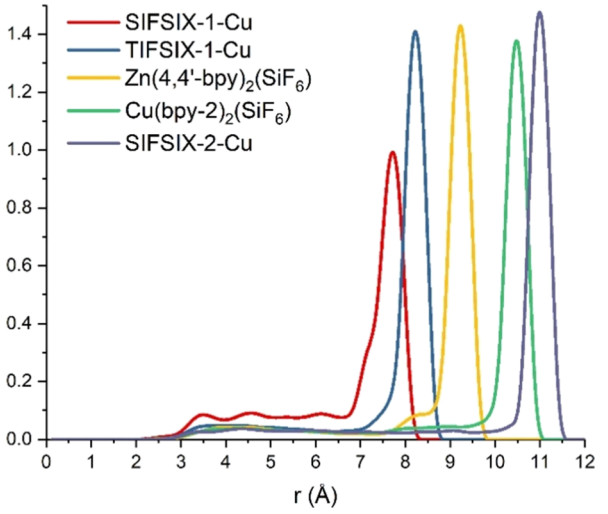

Figure 7. PSD plots of MOFs functionalized with fluorinated anions.

under study, we observe a strong peak at around 1.7 Å, suggesting direct binding between fluorine anions and PFOA, thanks to large partial negative charge on the fluorine atoms. Water also shows similar binding with a smaller amplitude of RDF, suggesting weaker interactions. Analysis of other RDF plots did not show any distinct adsorption sites for either PFOA or water.

Analysis of PSD and RDF together allowed for deriving an important conclusion. Neither too narrow nor too wide PSD show high HLC values despite their major RDF peak height suggesting strong affinity to the PFOA (Figure 8), highlighting the importance of topology in PFOA capture in aqueous media. We find that HLC shows the highest value in the pore diameters ranging 8–9 Å (Figure 2 and Table 3).

3.4. MOFs Functionalized with Trifluoromethyl Substitution. Another method to functionalize MOFs is employing trifluoromethyl substitution. In this category, we study $Zn(C_{17}H_8F_6O_4)$ and FMOF-1. Similar to the previous section, we investigate the impact of functionalization by computing HLCs, PSD, and RDF. The HLCs of water and PFOA in this MOF group are lower than the previous ones (Table 3). These two MOFs are more hydrophobic compared to those functionalized with fluorinated anions, but at the same time, the HLCs of PFOA are also low due to the narrow pore sizes (Figure 9). Hence, the relative ratio of HLC_{PFOA}/HLC_{water} remains much lower than other MOFs (Figure 2).

RDF plots for MOFs functionalized with trifluoromethyl-substituted ligands are shown in Figure 10. We observe that in $Zn(C_{17}H_8F_6O_4)$, PFOA prefers the fluorinated pores (Figure 10a, RDF plot for F-H_O), and water prefers the non-fluorinated pores, where ligands have hydrogens (Figure 10a, RDF plot for H-O_W). This is further supported by the F-H_W RDF plot (Figure 10a), which shows that the water molecules remain far away from the fluorine atoms of the $Zn(C_{17}H_8F_6O_4)$. The broad nature of the peaks in the F-H_O and H-O_W RDF plots in $Zn(C_{17}H_8F_6O_4)$ is due to the heterogeneous nature of the pores, i.e., fully fluorinated or fully non-fluorinated pore sizes results in broadening of the RDFs. For instance, while the distance between the hydrogen of PFOA and the closest fluorine atom in the pore is around 3 Å, the distance with all other fluorine atoms in the same pores covers a range of approximately 3 to 7 Å (Figure S15), resulting in a broader peak distribution. In FMOF-1, on the other hand, all pores are

https://doi.org/10.1021/acs.jpcc.2c07737
J. Phys. Chem. C 2023, 127, 3204–3216

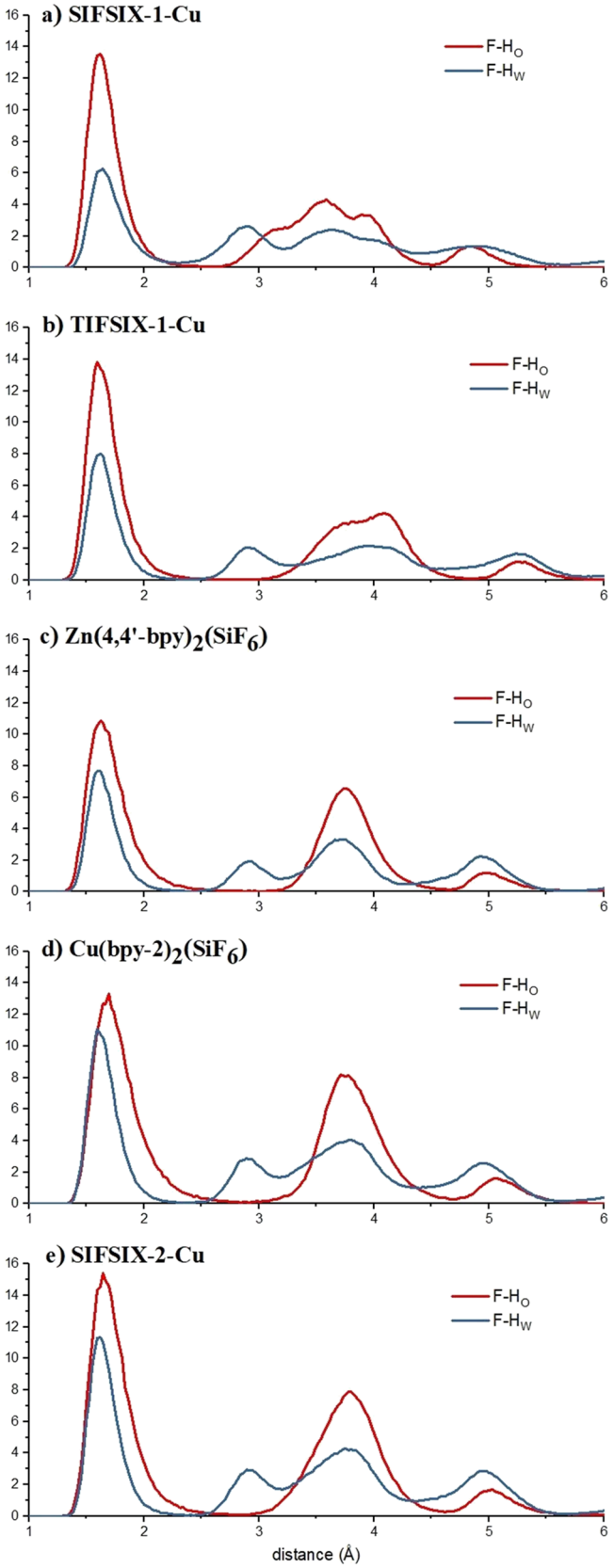

Figure 8. (a–e) RDF plots in MOFs that are functionalized with fluorine anions. F, fluorine atoms of MOFs; H_O, hydrogen of PFOA; and H_W, hydrogen of water. See Figure S14 for snapshots from simulations that illustrate the interactions between atom pairs for which RDF plots are shown here.

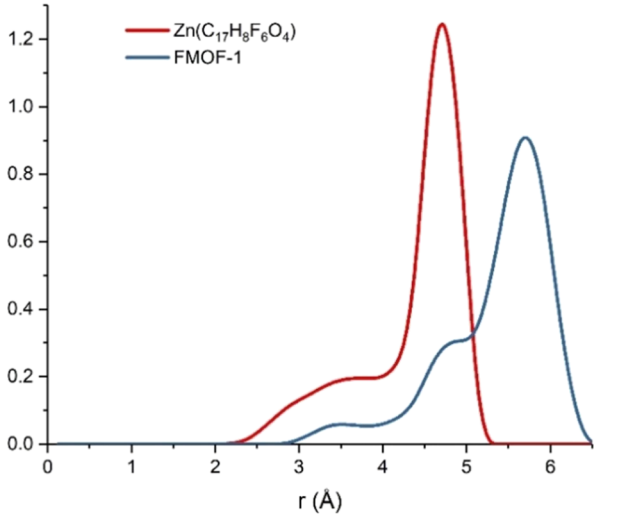

Figure 9. PSD plots of MOFs functionalized with trifluoromethyl-substituted ligands.

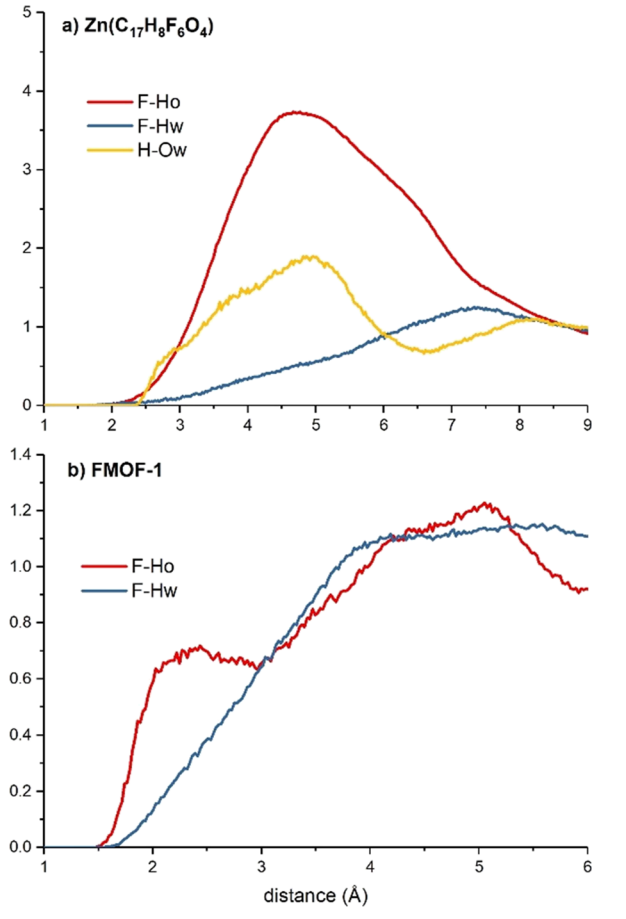

Figure 10. (a, b) RDF plots in MOFs functionalized with trifluoromethyl-substituted ligands. F, fluorine atoms of Zn-(C$_{17}$H$_8$F$_6$O$_4$) and FMOF-1; H, hydrogen atoms of Zn(C$_{17}$H$_8$F$_6$O$_4$); H_O, hydrogen atom of PFOA; H_W, hydrogen atoms of water; and O_W, oxygen atom of water. See Figures S15 and S16 for snapshots from simulations that illustrate the interactions between atom pairs for which RDF plots are shown in (a) and (b), respectively.

fluorinated; hence, this MOF has the lowest HLC for water. Therefore, RDF analysis did not reveal a preferred adsorption site for water (Figure 10b). In contrast, the hydrogen of PFOA

https://doi.org/10.1021/acs.jpcc.2c07737
J. Phys. Chem. C 2023, 127, 3204–3216

preferably interacts with fluorine of FMOF-1, as shown by the RDF plot of F-H_O in Figure 10b. Taken together, the low HLCs of PFOA in $Zn(C_{17}H_8F_6O_4)$ and FMOF-1 may be attributed to their narrow pores and lack of direct favorable interaction with the PFOA molecule.

3.5. MOFs Functionalized with Grafting of Perfluorinated Alkanes. In the MOFs considered in the previous sections, fluorine functionalization of the framework was achieved by chemical synthesis. However, MOFs can also be functionalized post-synthetically. One example of this kind is the perfluorinated alkane functionalization of NU-1000 through the SALI method.[68] Here, we consider the structure, denoted by NU-1000-PF, where the PFOA molecules were used as the source of the perfluoroalkyl chain that was covalently bonded to the terminal −OH group sites on the NU-1000 metal nodes by ligand incorporation reaction (Figure 11). The incorporation is an acid−base reaction, which occurs

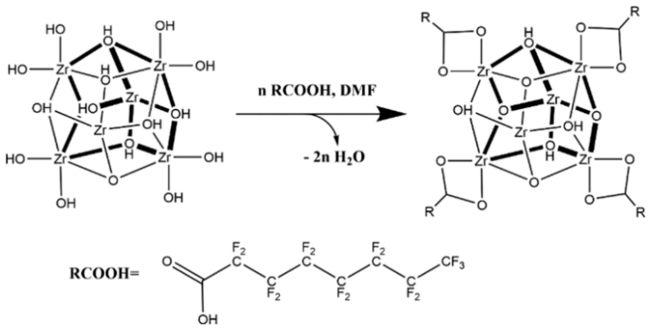

Figure 11. Solvent-assisted incorporation of PFOA ligands in NU-1000.

between the terminating hydroxyl groups on the Zr node of NU-1000 and the carboxylic acid group of PFOA molecules that gives water molecules as side product.

Table 3 gives the HLCs of PFOA and water for NU-1000 and NU-1000-PF. In Figure 2, we show the RH values. The PSD plots of these two structures are given in Figure 12. The R_H in NU-1000-PF is the highest among all the materials studied. The fairly good performance of NU-1000 is further improved upon fluorine functionalization (Figure 2). HLCs for water indicate only modest enhancement in hydrophobicity upon perfluoroalkane functionalization, in line with experimental findings.[68] They are in the order of 10^{-6} mol/kgPa, that is, the hydrophobicities of NU-1000 and NU-1000-PF are similar to those functionalized with trifluoromethyl and fluorine-substituted ligands (Table 3). For PFOA, however, the HLC is an order of magnitude higher in NU-1000-PF than NU-1000.

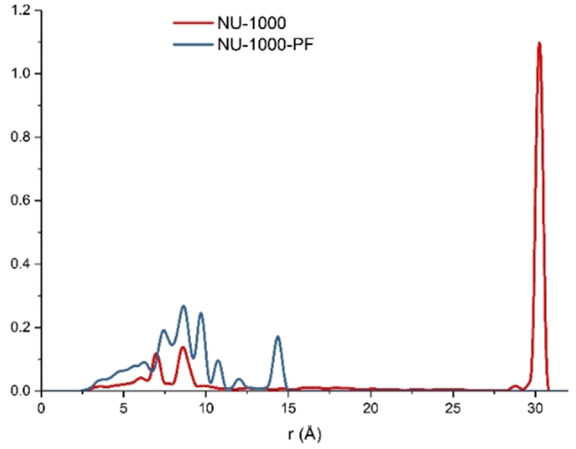

Figure 12. PSD plots of NU-1000 and its perfluoroalkyl functionalized version, NU-1000-PF.

Due to the incorporation of perfluoroalkyl chains, the size of the largest pore in NU-1000 reduces from ∼30 to ∼14 Å in NU-1000-PF, and both structures show narrower pores ranging from 7 to 9 Å. This may be attributed to stronger framework−PFOA interactions due to the relatively narrow pores of NU-1000-PF. RDF analysis provides more insights into the increase in HLC of PFOA after perfluoroalkane functionalization of NU-1000 (Figure 13 and Figure S17). In

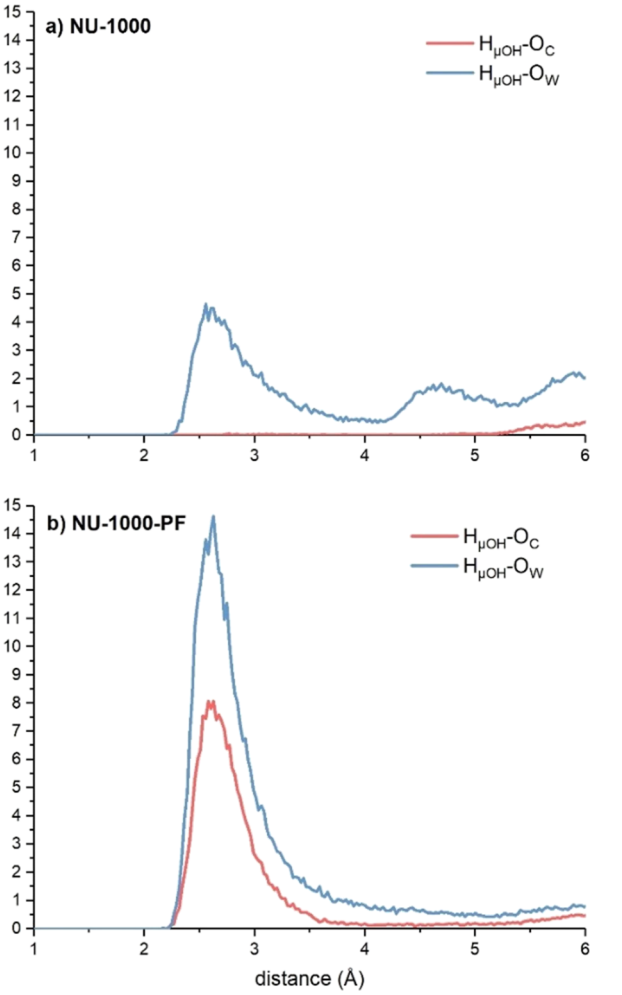

Figure 13. RDF plots in NU-1000 and NU-1000-PF. $H_{\mu OH}$, hydrogen atom of μOH sites in NU-1000 and NU-1000-PF; O_C, oxygen atom of PFOA double bonded to carbon; and O_W, oxygen atom of water. See Figures S19 and S20 for snapshots from simulations that illustrate the interactions between atom pairs for which RDF plots are shown here.

NU-1000, the PFOA molecule prefers to be adsorbed in the relatively narrow triangular pores, evidenced by the RDF plots for C-H_O and C-CF_3, where C is the carbon atoms on the ligands of NU-1000 and NU-1000-PF (Figure S17). Although the perfluoroalkyl chain has expectedly weak interactions, the carboxyl group serving as the hydrophilic head of PFOA does not interact strongly with any particular site. In contrast, μOH

https://doi.org/10.1021/acs.jpcc.2c07737
J. Phys. Chem. C 2023, 127, 3204−3216

is a preferred adsorption site for water molecules (Figure 13a, RDF plots for $H_{\mu OH}$-O_C and $H_{\mu OH}$-O_W). Interestingly, after perfluoroalkyl grafting, the μOH becomes a preferred adsorption site for PFOA, which is reflected by the peak observed in the RDF plot of $H_{\mu OH}$-O_C (Figure 13b). We observe that the so-called weak interactions between the fluorine atoms on the grafted perfluoroalkyl chains and those on PFOA were not found to play an important role (Figure S18). The emergence of $H_{\mu OH}$ as a new binding site for PFOA is also a factor in the increase of HLC of PFOA in NU-1000-PF compared to NU-1000. The intensity of the $H_{\mu OH}$-O_W peak in NU-1000-PF is higher compared to NU-1000, which is due to the decrease in the number of μOH sites as a result of the SALI reaction. It should be noted that although the atoms of the perfluoro-alkyl chain were fixed during the MC simulations, in reality, they are expected to be flexible and can affect the packing of PFOA molecules in the pores of NU-1000-PF during PFOA adsorption. However; we do not expect this flexibility to change our overall conclusion that NU-1000-PF has a higher affinity to PFOA than NU-1000.

4. CONCLUSIONS

Per- and polyfluoroalkyl substances (PFAS) are an emerging class of persistent polluters that do not break down in nature due to strong carbon−fluorine covalent bonds in their structures. PFAS has been detected in surface and groundwater sources, human urine, and serum samples. There are growing concerns about PFAS pollution as they have been linked to severe health issues. Adsorption by porous materials can be used to capture PFAS from water. In this respect, metal organic frameworks (MOFs) have been considered promising adsorbent materials. One strategy that can be used to develop MOFs to capture PFAS from water is functionalizing them with fluorine moieties. In this work, by using molecular simulations, we investigated different methods employed to design fluorine-functionalized MOF materials.

In this study, we considered three different fluorine functionalization methods: (i) incorporation of fluorinated anions as bridging ligands, (ii) trifluoromethyl or fluorine substitution of the ligands, and (iii) grafting of perfluorinated alkanes. Perfluorooctanoic acid (PFOA), one of the most widely encountered PFAS in water sources, was used as the probe molecule.

When we look at HLCs of the MOFs that are fluorine-functionalized with fluorinated anions (Table 3), two of them, TIFSIX-1-Cu and $Zn(4,4'\text{-bpy})_2(SiF_6)$, have the highest HLCs for PFOA among all the materials considered in this study. However, despite showing a strong affinity toward PFOA, they also show high HLC for water. They are relatively hydrophilic and may not be good at removing PFOA in water. The two trifluoromethyl functionalized MOFs considered here have the lowest HLCs for water (Table 3). On the other hand, they also have the lowest HLCs for the PFOA due to their narrow pores. MOFs functionalized with fluorine-substituted ligands exhibit high levels of hydrophobicity (Table 3); however, the HLCs for PFOA in these MOFs, even after complete fluorine substitution, are still not very high. The remaining three materials—NU-1000, its perfluoralkane grafted version NU-1000-PF, and zeolite Beta—do not have the highest HLCs for the PFOA, i.e., one to two orders of magnitude lower than those of for TIFSIX-1-Cu and $Zn(4,4'\text{-bpy})_2(SiF_6)$; however, they have the highest PFOA/water HLC ratio among all materials considered, i.e., in the order of 10.[10] Whereas, in $Zn(4,4'\text{-bpy})_2(SiF_6)$, the same ratio is in the order of 10.[9]

Our analysis of the 15 different kinds of MOFs reveals the following observations. The fluorination enhances the framework−PFOA interactions and serves as a viable strategy to remove PFAS from water resources. To effectively remove PFOA from water, the affinity of MOF to PFOA should be as large as possible, and conversely, its affinity for water should be as low as possible. The best performance can be achieved by creating hydrophobic pores. Due to the size of the PFOA, the topology of the pores also plays a crucial role. The MOFs that have pore sizes below 6 Å are too narrow to uptake PFOA. We found the ideal pore size that enhances PFOA removal to be 8−10 Å. This rationale can be used to identify and optimize porous materials for the removal of PFOA from water resources at very low concentrations of PFOA.

■ ASSOCIATED CONTENT

Supporting Information

The Supporting Information is available free of charge at https://pubs.acs.org/doi/10.1021/acs.jpcc.2c07737.

Structural representations of the MOFs included in this study; RDF plots (PDF)

■ AUTHOR INFORMATION

Corresponding Author

A. Ozgur Yazaydin − *Department of Chemical Engineering, University College London, London WC1E7JE, United Kingdom*; orcid.org/0000-0001-8562-723X; Email: ozgur.yazaydin@ucl.ac.uk

Authors

Turan Selman Erkal − *Department of Chemical Engineering, University College London, London WC1E7JE, United Kingdom*

Norazanita Shamsuddin − *Faculty of Integrated Technologies, Universiti Brunei Darussalam, Gadong BE1410, Brunei Darussalam*

Serdal Kirmizialtin − *Chemistry Program, Science Division, New York University, Abu Dhabi, United Arab Emirates*; orcid.org/0000-0001-8380-5725

Complete contact information is available at: https://pubs.acs.org/10.1021/acs.jpcc.2c07737

Author Contributions

The manuscript was written through contributions of all authors. All authors have given approval to the final version of the manuscript.

Notes

The authors declare no competing financial interest.

■ ACKNOWLEDGMENTS

The authors acknowledge the use of the UCL Myriad High Performance Computing Facility (Myriad@UCL), and associated support services, in the completion of this work.

■ REFERENCES

(1) Schwarzenbach, R. P.; Egli, T.; Hofstetter, T. B.; Von Gunten, U.; Wehrli, B. Global Water Pollution and Human Health. *Annual Review of Environment and Resources* **2010**, *35*, 109−136.

(2) Posthuma, L.; Zijp, M. C.; De Zwart, D.; Van de Meent, D.; Globevnik, L.; Koprivsek, M.; Focks, A.; Van Gils, J.; Birk, S.

Chemical Pollution Imposes Limitations to the Ecological Status of European Surface Waters. *Sci. Rep.* **2020**, *10*, 14825.
(3) Moody, C. A.; Field, J. A. Perfluorinated Surfactants and the Environmental Implications of Their Use in Fire-Fighting Foams. *Environ. Sci. Technol.* **2000**, *34*, 3864−3870.
(4) Dixit, F.; Barbeau, B.; Mostafavi, S. G.; Mohseni, M. Pfoa and Pfos Removal by Ion Exchange for Water Reuse and Drinking Applications: Role of Organic Matter Characteristics. *Environ. Sci.: Water Res. Technol.* **2019**, *5*, 1782−1795.
(5) Pilli, S.; Pandey, A. K.; Pandey, V.; Pandey, K.; Muddam, T.; Thirunagari, B. K.; Thota, S. T.; Varjani, S.; Tyagi, R. D. Detection and Removal of Poly and Perfluoroalkyl Polluting Substances for Sustainable Environment. *J. Environ. Manage.* **2021**, *297*, 113336.
(6) Trager, R. A Persistent Perfluorinated Problem. *Chem. World* **2019**, *2019*, 26−17.
(7) Garg, S.; Wang, J.; Kumar, P.; Mishra, V.; Arafat, H.; Sharma, R. S.; Dumée, L. F. Remediation of Water from Per-/Poly-Fluoroalkyl Substances (Pfas) − Challenges and Perspectives. *J. Environ. Chem. Eng.* **2021**, *9*, 105784.
(8) Hale, S. E.; Arp, H. P. H.; Schliebner, I.; Neumann, M. What's in a Name: Persistent, Mobile, and Toxic (Pmt) and Very Persistent and Very Mobile (Vpvm) Substances. *Environ. Sci. Technol.* **2020**, *54*, 14790−14792.
(9) Brendel, S.; Fetter, É.; Staude, C.; Vierke, L.; Biegel-Engler, A. Short-Chain Perfluoroalkyl Acids: Environmental Concerns and a Regulatory Strategy under Reach. *Environ. Sci. Eur.* **2018**, *30*, 9.
(10) Cousins, I. T.; DeWitt, J. C.; Glüge, J.; Goldenman, G.; Herzke, D.; Lohmann, R.; Ng, C. A.; Scheringer, M.; Wang, Z. The High Persistence of Pfas Is Sufficient for Their Management as a Chemical Class. *Environ. Sci.: Processes Impacts* **2020**, *22*, 2307−2312.
(11) Brusseau, M. L.; Anderson, R. H.; Guo, B. Pfas Concentrations in Soils: Background Levels Versus Contaminated Sites. *Sci. Total Environ.* **2020**, *740*, 140017.
(12) Igarashi, Y.; Takahashi, M.; Tsutsumi, T.; Inoue, K.; Akiyama, H. Monitoring Analysis of Perfluoroalkyl Substances and F-53b in Bottled Water, Tea and Juice Samples by Lc-Ms/Ms. *Chem. Pharm. Bull.* **2021**, *69*, 286−290.
(13) Hu, X. C.; Andrews, D. Q.; Lindstrom, A. B.; Bruton, T. A.; Schaider, L. A.; Grandjean, P.; Lohmann, R.; Carignan, C. C.; Blum, A.; Balan, S. A.; et al. Detection of Poly- and Perfluoroalkyl Substances (Pfass) in U.S. Drinking Water Linked to Industrial Sites, Military Fire Training Areas, and Wastewater Treatment Plants. *Environ. Sci. Technol. Lett.* **2016**, *3*, 344−350.
(14) Guardian, M. G. E.; Boongaling, E. G.; Bernardo-Boongaling, V. R. R.; Gamonchuang, J.; Boontongto, T.; Burakham, R.; Arnnok, P.; Aga, D. S. Prevalence of Per- and Polyfluoroalkyl Substances (Pfass) in Drinking and Source Water from Two Asian Countries. *Chemosphere* **2020**, *256*, 127115.
(15) Ingelido, A. M.; Abballe, A.; Gemma, S.; Dellatte, E.; Iacovella, N.; De Angelis, G.; Zampaglioni, F.; Marra, V.; Miniero, R.; Valentini, S.; et al. Biomonitoring of Perfluorinated Compounds in Adults Exposed to Contaminated Drinking Water in the Veneto Region, Italy. *Environ. Int.* **2018**, *110*, 149−159.
(16) Banzhaf, S.; Filipovic, M.; Lewis, J.; Sparrenbom, C. J.; Barthel, R. A Review of Contamination of Surface-, Ground-, and Drinking Water in Sweden by Perfluoroalkyl and Polyfluoroalkyl Substances (Pfass). *Ambio* **2017**, *46*, 335−346.
(17) Cousins, I. T.; Johansson, J. H.; Salter, M. E.; Sha, B.; Scheringer, M. Outside the Safe Operating Space of a New Planetary Boundary for Per- and Polyfluoroalkyl Substances (Pfas). *Environ. Sci. Technol.* **2022**, *56*, 11172−11179.
(18) Calafat, A. M.; Wong, L.-Y.; Kuklenyik, Z.; Reidy, J. A.; Needham, L. L. Polyfluoroalkyl Chemicals in the U.S. Population: Data from the National Health and Nutrition Examination Survey (Nhanes) 2003-2004 and Comparisons with Nhanes 1999-2000. *Environ. Health Perspect.* **2007**, *115*, 1596−1602.
(19) Hekster, F. M.; Laane, R. W. P. M.; de Voogt, P., Environmental and Toxicity Effects of Perfluoroalkylated Substances. In *Reviews of Environmental Contamination and Toxicology*, SpringerNew York: New York, NY, 2003; pp. 99−121.
(20) Wang, Z.; Cousins, I. T.; Scheringer, M.; Hungerbuehler, K. Hazard Assessment of Fluorinated Alternatives to Long-Chain Perfluoroalkyl Acids (Pfaas) and Their Precursors: Status Quo, Ongoing Challenges and Possible Solutions. *Environ. Int.* **2015**, *75*, 172−179.
(21) Gaballah, S.; Swank, A.; Sobus, J. R.; Howey, X. M.; Schmid, J.; Catron, T.; McCord, J.; Hines, E.; Strynar, M.; Tal, T. Evaluation of Developmental Toxicity, Developmental Neurotoxicity, and Tissue Dose in Zebrafish Exposed to Genx and Other Pfas. *Environ. Health Perspect.* **2020**, *128*, No. 047005.
(22) Sinclair, G. M.; Long, S. M.; Jones, O. A. H. What Are the Effects of Pfas Exposure at Environmentally Relevant Concentrations? *Chemosphere* **2020**, *258*, 127340.
(23) Barry, V.; Winquist, A.; Steenland, K. Perfluorooctanoic Acid (Pfoa) Exposures and Incident Cancers among Adults Living near a Chemical Plant. *Environ. Health Perspect.* **2013**, *121*, 1313−1318.
(24) Fenton, S. E.; Ducatman, A.; Boobis, A.; DeWitt, J. C.; Lau, C.; Ng, C.; Smith, J. S.; Roberts, S. M. Per- and Polyfluoroalkyl Substance Toxicity and Human Health Review: Current State of Knowledge and Strategies for Informing Future Research. *Environ. Toxicol. Chem.* **2021**, *40*, 606−630.
(25) Romano, M. E.; Xu, Y.; Calafat, A. M.; Yolton, K.; Chen, A.; Webster, G. M.; Eliot, M. N.; Howard, C. R.; Lanphear, B. P.; Braun, J. M. Maternal Serum Perfluoroalkyl Substances During Pregnancy and Duration of Breastfeeding. *Environ. Res.* **2016**, *149*, 239−246.
(26) Timmermann, C. A. G.; Budtz-Jørgensen, E.; Petersen, M. S.; Weihe, P.; Steuerwald, U.; Nielsen, F.; Jensen, T. K.; Grandjean, P. Shorter Duration of Breastfeeding at Elevated Exposures to Perfluoroalkyl Substances. *Reprod. Toxicol.* **2017**, *68*, 164−170.
(27) Rosen, E. M.; Brantsæter, A. L.; Carroll, R.; Haug, L.; Singer, A. B.; Zhao, S.; Ferguson, K. K. Maternal Plasma Concentrations of Per- and Polyfluoroalkyl Substances and Breastfeeding Duration in the Norwegian Mother and Child Cohort. *Environ. Epidemiol.* **2018**, *2*, No. e027.
(28) Bonefeld-Jørgensen, E. C.; Long, M.; Fredslund, S. O.; Bossi, R.; Olsen, J. Breast Cancer Risk after Exposure to Perfluorinated Compounds in Danish Women: A Case−Control Study Nested in the Danish National Birth Cohort. *Cancer, Causes Control* **2014**, *25*, 1439−1448.
(29) Dickman, R. A.; Aga, D. S. A Review of Recent Studies on Toxicity, Sequestration, and Degradation of Per- and Polyfluoroalkyl Substances (Pfas). *J. Hazard. Mater.* **2022**, *436*, 129120.
(30) Guardian, M. G. E.; Antle, J. P.; Vexelman, P. A.; Aga, D. S.; Simpson, S. M. Resolving Unknown Isomers of Emerging Per- and Polyfluoroalkyl Substances (Pfass) in Environmental Samples Using Cosmo-Rs-Derived Retention Factor and Mass Fragmentation Patterns. *J. Hazard. Mater.* **2021**, *402*, 123478.
(31) Getzinger, G. J.; Ferguson, P. L. High-Throughput Trace-Level Suspect Screening for Per- and Polyfluoroalkyl Substances in Environmental Waters by Peak-Focusing Online Solid Phase Extraction and High-Resolution Mass Spectrometry. *ACS ES&T Water* **2021**, *1*, 1240−1251.
(32) Koelmel, J. P.; Paige, M. K.; Aristizabal-Henao, J. J.; Robey, N. M.; Nason, S. L.; Stelben, P. J.; Li, Y.; Kroeger, N. M.; Napolitano, M. P.; Savvaides, T.; et al. Toward Comprehensive Per- and Polyfluoroalkyl Substances Annotation Using Fluoromatch Software and Intelligent High-Resolution Tandem Mass Spectrometry Acquisition. *Anal. Chem.* **2020**, *92*, 11186−11194.
(33) Li, P.; Zhi, D.; Zhang, X.; Zhu, H.; Li, Z.; Peng, Y.; He, Y.; Luo, L.; Rong, X.; Zhou, Y. Research Progress on the Removal of Hazardous Perfluorochemicals: A Review. *J. Environ. Manage.* **2019**, *250*, 109488.
(34) Trojanowicz, M.; Bojanowska-Czajka, A.; Bartosiewicz, I.; Kulisa, K. Advanced Oxidation/Reduction Processes Treatment for Aqueous Perfluorooctanoate (Pfoa) and Perfluorooctanesulfonate (Pfos) − a Review of Recent Advances. *Chem. Eng. J.* **2018**, *336*, 170−199.

https://doi.org/10.1021/acs.jpcc.2c07737
J. Phys. Chem. C 2023, 127, 3204−3216

(35) Yang, L.; He, L.; Xue, J.; Ma, Y.; Xie, Z.; Wu, L.; Huang, M.; Zhang, Z. Persulfate-Based Degradation of Perfluorooctanoic Acid (Pfoa) and Perfluorooctane Sulfonate (Pfos) in Aqueous Solution: Review on Influences, Mechanisms and Prospective. *J. Hazard. Mater.* **2020**, *393*, 122405.
(36) Flores, C.; Ventura, F.; Martin-Alonso, J.; Caixach, J. Occurrence of Perfluorooctane Sulfonate (Pfos) and Perfluorooctanoate (Pfoa) in N.E. Spanish Surface Waters and Their Removal in a Drinking Water Treatment Plant That Combines Conventional and Advanced Treatments in Parallel Lines. *Sci. Total Environ.* **2013**, *461-462*, 618−626.
(37) Bao, Y.; Niu, J.; Xu, Z.; Gao, D.; Shi, J.; Sun, X.; Huang, Q. Removal of Perfluorooctane Sulfonate (Pfos) and Perfluorooctanoate (Pfoa) from Water by Coagulation: Mechanisms and Influencing Factors. *J. Colloid Interface Sci.* **2014**, *434*, 59−64.
(38) Rahman, M. F.; Peldszus, S.; Anderson, W. B. Behaviour and Fate of Perfluoroalkyl and Polyfluoroalkyl Substances (Pfass) in Drinking Water Treatment: A Review. *Water Res.* **2014**, *50*, 318−340.
(39) Liu, L.; Liu, Y.; Gao, B.; Ji, R.; Li, C.; Wang, S. Removal of Perfluorooctanoic Acid (Pfoa) and Perfluorooctane Sulfonate (Pfos) from Water by Carbonaceous Nanomaterials: A Review. *Crit. Rev. Environ. Sci. Technol.* **2020**, *50*, 2379−2414.
(40) Wang, R.; Ching, C.; Dichtel, W. R.; Helbling, D. E. Evaluating the Removal of Per- and Polyfluoroalkyl Substances from Contaminated Groundwater with Different Adsorbents Using a Suspect Screening Approach. *Environ. Sci. Technol. Lett.* **2020**, *7*, 954−960.
(41) Ateia, M.; Alsbaiee, A.; Karanfil, T.; Dichtel, W. Efficient Pfas Removal by Amine-Functionalized Sorbents: Critical Review of the Current Literature. *Environ. Sci. Technol. Lett.* **2019**, *6*, 688−695.
(42) Xu, C.; Chen, H.; Jiang, F. Adsorption of Perflurooctane Sulfonate (Pfos) and Perfluorooctanoate (Pfoa) on Polyaniline Nanotubes. *Colloids Surf., A* **2015**, *479*, 60−67.
(43) Skorjanc, T.; Shetty, D.; Trabolsi, A. Pollutant Removal with Organic Macrocycle-Based Covalent Organic Polymers and Frameworks. *Chem* **2021**, *7*, 882−918.
(44) Shetty, D.; Jahović, I.; Skorjanc, T.; Erkal, T. S.; Ali, L.; Raya, J.; Asfari, Z.; Olson, M. A.; Kirmizialtin, S.; Yazaydin, A. O.; et al. Rapid and Efficient Removal of Perfluorooctanoic Acid from Water with Fluorine-Rich Calixarene-Based Porous Polymers. *ACS Appl. Mater. Interfaces* **2020**, *12*, 43160−43166.
(45) Xiao, L.; Ling, Y.; Alsbaiee, A.; Li, C.; Helbling, D. E.; Dichtel, W. R. B-Cyclodextrin Polymer Network Sequesters Perfluorooctanoic Acid at Environmentally Relevant Concentrations. *J. Am. Chem. Soc.* **2017**, *139*, 7689−7692.
(46) Van den Bergh, M.; Krajnc, A.; Voorspoels, S.; Tavares, S. R.; Mullens, S.; Beurroies, I.; Maurin, G.; Mali, G.; De Vos, D. E. Highly Selective Removal of Perfluorinated Contaminants by Adsorption on All-Silica Zeolite Beta. *Angew. Chem.* **2020**, *59*, 14086−14090.
(47) Ochoa-Herrera, V.; Sierra-Alvarez, R. Removal of Perfluorinated Surfactants by Sorption onto Granular Activated Carbon, Zeolite and Sludge. *Chemosphere* **2008**, *72*, 1588−1593.
(48) Wang, W.; Zhou, Z.; Shao, H.; Zhou, S.; Yu, G.; Deng, S. Cationic Covalent Organic Framework for Efficient Removal of Pfoa Substitutes from Aqueous Solution. *Chem. Eng. J.* **2021**, *412*, 127509.
(49) Ji, W.; Xiao, L.; Ling, Y.; Ching, C.; Matsumoto, M.; Bisbey, R. P.; Helbling, D. E.; Dichtel, W. R. Removal of Genx and Perfluorinated Alkyl Substances from Water by Amine-Functionalized Covalent Organic Frameworks. *J. Am. Chem. Soc.* **2018**, *140*, 12677−12681.
(50) Wang, B.; Lee, L. S.; Wei, C.; Fu, H.; Zheng, S.; Xu, Z.; Zhu, D. Covalent Triazine-Based Framework: A Promising Adsorbent for Removal of Perfluoroalkyl Acids from Aqueous Solution. *Environ. Pollut.* **2016**, *216*, 884−892.
(51) Sini, K.; Bourgeois, D.; Idouhar, M.; Carboni, M.; Meyer, D. Metal−Organic Framework Sorbents for the Removal of Perfluorinated Compounds in an Aqueous Environment. *New J. Chem.* **2018**, *42*, 17889−17894.
(52) Chen, M.-J.; Yang, A.-C.; Wang, N.-H.; Chiu, H.-C.; Li, Y.-L.; Kang, D.-Y.; Lo, S.-L. Influence of Crystal Topology and Interior Surface Functionality of Metal-Organic Frameworks on Pfoa Sorption Performance. *Microporous Mesoporous Mater.* **2016**, *236*, 202−210.
(53) Li, R.; Alomari, S.; Stanton, R.; Wasson, M. C.; Islamoglu, T.; Farha, O. K.; Holsen, T. M.; Thagard, S. M.; Trivedi, D. J.; Wriedt, M. Efficient Removal of Per- and Polyfluoroalkyl Substances from Water with Zirconium-Based Metal−Organic Frameworks. *Chem. Mater.* **2021**, *33*, 3276−3285.
(54) Liu, K.; Zhang, S.; Hu, X.; Zhang, K.; Roy, A.; Yu, G. Understanding the Adsorption of Pfoa on Mil-101(Cr)-Based Anionic-Exchange Metal−Organic Frameworks: Comparing Dft Calculations with Aqueous Sorption Experiments. *Environ. Sci. Technol.* **2015**, *49*, 8657−8665.
(55) Tan, X.; Zhong, J.; Fu, C.; Dang, H.; Han, Y.; Král, P.; Guo, J.; Yuan, Z.; Peng, H.; Zhang, C.; et al. Amphiphilic Perfluoropolyether Copolymers for the Effective Removal of Polyfluoroalkyl Substances from Aqueous Environments. *Macromolecules* **2021**, *54*, 3447−3457.
(56) Chen, P.-Y.; Wang, B.; Zhuang, S.; Chen, Y.; Wei, Y.-P. Polyacrylonitrile Fiber Functionalized with Fluorous Hyperbranched Polyethylenimine for Selective Removal of Perfluorooctane Sulfonate (Pfos) in Firefighting Wastewaters. *Colloids Surf., A* **2021**, *619*, 126539.
(57) Wang, W.; Xu, Z.; Zhang, X.; Wimmer, A.; Shi, E.; Qin, Y.; Zhao, X.; Zhou, B.; Li, L. Rapid and Efficient Removal of Organic Micropollutants from Environmental Water Using a Magnetic Nanoparticles-Attached Fluorographene-Based Sorbent. *Chem. Eng. J.* **2018**, *343*, 61−68.
(58) Noro, S.-i.; Nakamura, T. Fluorine-Functionalized Metal−Organic Frameworks and Porous Coordination Polymers. *NPG Asia Mater.* **2017**, *9*, e433−e433.
(59) Subramanian, S.; Zaworotko, M. J. Porous Solids by Design: [Zn(4,4′-Bpy)2(Sif6)]N·Xdmf, a Single Framework Octahedral Coordination Polymer with Large Square Channels. *Angew. Chem., Int. Ed. Engl.* **1995**, *34*, 2127−2129.
(60) Nugent, P.; Belmabkhout, Y.; Burd, S. D.; Cairns, A. J.; Luebke, R.; Forrest, K.; Pham, T.; Ma, S.; Space, B.; Wojtas, L.; et al. Porous Materials with Optimal Adsorption Thermodynamics and Kinetics for Co2 Separation. *Nature* **2013**, *495*, 80−84.
(61) Nugent, P.; Rhodus, V.; Pham, T.; Tudor, B.; Forrest, K.; Wojtas, L.; Space, B.; Zaworotko, M. Enhancement of Co2 Selectivity in a Pillared Pcu Mom Platform through Pillar Substitution. *Chem. Commun.* **2013**, *49*, 1606−1608.
(62) Burd, S. D.; Ma, S.; Perman, J. A.; Sikora, B. J.; Snurr, R. Q.; Thallapally, P. K.; Tian, J.; Wojtas, L.; Zaworotko, M. J. Highly Selective Carbon Dioxide Uptake by [Cu(Bpy-N)2(Sif6)] (Bpy-1 = 4,4′-Bipyridine; Bpy-2 = 1,2-Bis(4-Pyridyl)Ethene). *J. Am. Chem. Soc.* **2012**, *134*, 3663−3666.
(63) Cui, X.; Chen, K.; Xing, H.; Yang, Q.; Krishna, R.; Bao, Z.; Wu, H.; Zhou, W.; Dong, X.; Han, Y.; et al. Pore Chemistry and Size Control in Hybrid Porous Materials for Acetylene Capture from Ethylene. *Science* **2016**, *353*, 141−144.
(64) Noro, S. I.; Kitagawa, S.; Kondo, M.; Seki, K. A New, Methane Adsorbent, Porous Coordination Polymer [{Cusif6(4,4′-Bipyridine)-2}N]. *Angew. Chem., Int. Ed.* **2000**, *39*, 2081−2084.
(65) Monge, A.; Snejko, N.; Gutiérrez-Puebla, E.; Medina, M.; Cascales, C.; Ruiz-Valero, C.; Iglesias, M.; Gómez-Lor, B. One Teflon®-Like Channelled Nanoporous Polymer with a Chiral and New Uninodal 4-Connected Net: Sorption and Catalytic Properties. *Chem. Commun.* **2005**, 1291−1293.
(66) Yang, C.; Kaipa, U.; Mather, Q. Z.; Wang, X.; Nesterov, V.; Venero, A. F.; Omary, M. A. Fluorous Metal−Organic Frameworks with Superior Adsorption and Hydrophobic Properties toward Oil Spill Cleanup and Hydrocarbon Storage. *J. Am. Chem. Soc.* **2011**, *133*, 18094−18097.
(67) Piscopo, C. G.; Trapani, F.; Polyzoidis, A.; Schwarzer, M.; Pace, A.; Loebbecke, S. Positive Effect of the Fluorine Moiety on the Oxygen Storage Capacity of Uio-66 Metal−Organic Frameworks. *New J. Chem.* **2016**, *40*, 8220−8224.
(68) Deria, P.; Mondloch, J. E.; Tylianakis, E.; Ghosh, P.; Bury, W.; Snurr, R. Q.; Hupp, J. T.; Farha, O. K. Perfluoroalkane

Functionalization of Nu-1000 Via Solvent-Assisted Ligand Incorporation: Synthesis and Co2 Adsorption Studies. *J. Am. Chem. Soc.* **2013**, *135*, 16801−16804.
(69) DeChellis, D. M.; Ngule, C. M.; Genna, D. T. Removal of Hydrocarbon Contaminants from Water with Perfluorocarboxylated Uio-6x Derivatives. *J. Mater. Chem. A* **2020**, *8*, 5848−5852.
(70) Stelzer, J.; Paulus, M.; Hunger, M.; Weitkamp, J. Hydrophobic Properties of All-Silica Zeolite Beta. *Microporous Mesoporous Mater.* **1998**, *22*, 1−8.
(71) Groom, C. R.; Bruno, I. J.; Lightfoot, M. P.; Ward, S. C. The Cambridge Structural Database. *Acta Crystallogr., Sect. B: Struct. Sci., Cryst. Eng. Mater.* **2016**, *72*, 171−179.
(72) Segall, M. D.; Lindan, P. J. D.; Probert, M. J.; Pickard, C. J.; Hasnip, P. J.; Clark, S. J.; Payne, M. C. First-Principles Simulation: Ideas, Illustrations and the Castep Code. *J. Phys.: Condens. Matter* **2002**, *14*, 2717−2744.
(73) Campañá, C.; Mussard, B.; Woo, T. K. Electrostatic Potential Derived Atomic Charges for Periodic Systems Using a Modified Error Functional. *J. Chem. Theory Comput.* **2009**, *5*, 2866−2878.
(74) Rappe, A. K.; Casewit, C. J.; Colwell, K. S.; Goddard, W. A.; Skiff, W. M. Uff, a Full Periodic Table Force Field for Molecular Mechanics and Molecular Dynamics Simulations. *J. Am. Chem. Soc.* **1992**, *114*, 10024−10035.
(75) Bai, P.; Tsapatsis, M.; Siepmann, J. I. Trappe-Zeo: Transferable Potentials for Phase Equilibria Force Field for All-Silica Zeolites. *J. Phys. Chem. C* **2013**, *117*, 24375−24387.
(76) Horn, H. W.; Swope, W. C.; Pitera, J. W.; Madura, J. D.; Dick, T. J.; Hura, G. L.; Head-Gordon, T. Development of an Improved Four-Site Water Model for Biomolecular Simulations: Tip4p-Ew. *J. Chem. Phys.* **2004**, *120*, 9665−9678.
(77) Zhang, L.; Siepmann, J. I. Pressure Dependence of the Vapor−Liquid−Liquid Phase Behavior in Ternary Mixtures Consisting of N-Alkanes, N-Perfluoroalkanes, and Carbon Dioxide. *J. Phys. Chem. B* **2005**, *109*, 2911−2919.
(78) Potoff, J. J.; Bernard-Brunel, D. A. Mie Potentials for Phase Equilibria Calculations: Application to Alkanes and Perfluoroalkanes. *J. Phys. Chem. B* **2009**, *113*, 14725−14731.
(79) Stubbs, J. M.; Potoff, J. J.; Siepmann, J. I. Transferable Potentials for Phase Equilibria. 6. United-Atom Description for Ethers, Glycols, Ketones, and Aldehydes. *J. Phys. Chem. B* **2004**, *108*, 17596−17605.
(80) Chen, B.; Potoff, J. J.; Siepmann, J. I. Monte Carlo Calculations for Alcohols and Their Mixtures with Alkanes. Transferable Potentials for Phase Equilibria. 5. United-Atom Description of Primary, Secondary, and Tertiary Alcohols. *J. Phys. Chem. B* **2001**, *105*, 3093−3104.
(81) Kamath, G.; Cao, F.; Potoff, J. J. An Improved Force Field for the Prediction of the Vapor−Liquid Equilibria for Carboxylic Acids. *J. Phys. Chem. B* **2004**, *108*, 14130−14136.
(82) Loganathan, N.; Wilson, A. K. Adsorption, Structure, and Dynamics of Short- and Long-Chain Pfas Molecules in Kaolinite: Molecular-Level Insights. *Environ. Sci. Technol.* **2022**, *56*, 8043−8052.
(83) Choudhary, A.; Dong, D.; Tsianou, M.; Alexandridis, P.; Bedrov, D. Adsorption Mechanism of Perfluorooctanoate on Cyclodextrin-Based Polymers: Probing the Synergy of Electrostatic and Hydrophobic Interactions with Molecular Dynamics Simulations. *ACS Mater. Lett.* **2022**, *4*, 853−859.
(84) Dubbeldam, D.; Calero, S.; Ellis, D. E.; Snurr, R. Q. Raspa: Molecular Simulation Software for Adsorption and Diffusion in Flexible Nanoporous Materials. *Mol. Simul.* **2016**, *42*, 81−101.
(85) Widom, B. Some Topics in the Theory of Fluids. *J. Chem. Phys.* **1963**, *39*, 2808−2812.
(86) Bonato, M.; Corrà, F.; Bellio, M.; Guidolin, L.; Tallandini, L.; Irato, P.; Santovito, G. Pfas Environmental Pollution and Antioxidant Responses: An Overview of the Impact on Human Field. *Int. J. Environ. Res. Public Health* **2020**, *17*, 8020.
(87) Emmett, E. A.; Shofer, F. S.; Zhang, H.; Freeman, D.; Desai, C.; Shaw, L. M. Community Exposure to Perfluorooctanoate: Relationships between Serum Concentrations and Exposure Sources. *J. Occup. Environ. Med.* **2006**, *48*, 759−770.
(88) Post, G. B.; Cohn, P. D.; Cooper, K. R. Perfluorooctanoic Acid (Pfoa), an Emerging Drinking Water Contaminant: A Critical Review of Recent Literature. *Environ. Res.* **2012**, *116*, 93−117.
(89) Post, G. B.; Louis, J. B.; Cooper, K. R.; Boros-Russo, B. J.; Lippincott, R. L. Occurrence and Potential Significance of Perfluorooctanoic Acid (Pfoa) Detected in New Jersey Public Drinking Water Systems. *Environ. Sci. Technol.* **2009**, *43*, 4547−4554.
(90) Sarkisov, L.; Harrison, A. Computational Structure Characterisation Tools in Application to Ordered and Disordered Porous Materials. *Mol. Simul.* **2011**, *37*, 1248−1257.

NOTE ADDED AFTER ASAP PUBLICATION

This paper was published ASAP on February 3, 2023, with incorrect reference numbers in Table 2. The corrected version was reposted on February 16, 2023.

https://doi.org/10.1021/acs.jpcc.2c07737
J. Phys. Chem. C 2023, 127, 3204−3216